LIMNOLOGY and OCEANOGRAPHY

ASLO

*Limnol. Oceanogr.* 60, 2014, 29–41

doi: 10.1002/lno.10008

# Dissipation and mixing during the onset of stratification in a temperate lake, Windermere

**John H. Simpson,[1]* Natasha S. Lucas,[1] Ben Powell,[1] Stephen C. Maberly[2]**
[1]Bangor University School of Ocean Sciences, Menai Bridge, Anglesey, United Kingdom
[2]Lake Ecosystems Group, Centre for Ecology and Hydrology, Lancaster Environment Centre, Lancaster, United Kingdom

## *Abstract*

Acoustic Doppler Current Profilers and chains of temperature sensors were used to observe the spring transition to stable stratification over a 55-d period in a temperate lake. Observations of the flow structure were complemented by measurements of dissipation, based on the structure function method, near the lake bed and in the upper part of the water column. During complete vertical mixing, wind-driven motions had horizontally isotropic velocities with roughly equal barotropic and baroclinic kinetic energy. Dissipation was closely correlated with the wind-speed cubed, indicating law of the wall scaling, and had peak values of $\sim 1 \times 10^{-5.5}$ W kg$^{-1}$ at ten meters depth during maximum wind forcing ($W \sim 15$ m s$^{-1}$). As stratification developed, the flow evolved into a predominantly baroclinic regime dominated by the first mode internal seiche, with root mean square axial flow speeds of $\sim$ 2–3 cm$^{-1}$; $\sim$ 2.5–times the transverse component. At 2.8 m above the bed, most of the dissipation occurred in a number of strong maxima coinciding with peaks of near-bed flow. In the pycnocline, dissipation was low most of the time, but with pronounced maxima (reaching $\sim 1 \times 10^{-5}$ W kg$^{-1}$) closely related to the local velocity shear. The downward diffusive heat flux across the pycnocline over 27.5 d accounted for $\sim$ 70% of the temperature rise in the water column below. Total lake kinetic energy increased by a factor of three between mixed and stratified regimes, in spite of reduced wind forcing, indicating less efficient damping in stable conditions.

Stratification in lakes and oceans has a major effect on their physics, chemistry, and biology. Vertical mixing is a vital component of the physical processes which, in large part, are responsible for controlling biogeochemical fluxes in aquatic systems. Forcing by wind-stress at the water surface is the primary source of energy that drives the mixing with additional inputs from convective motions during periods of surface cooling (Wuest and Lorke 2003). In the vertically mixed regime, which prevails during winter months, momentum can penetrate readily through the water column and drive stirring down to the bed in all but the deepest lakes. Soon after the onset of seasonal heating in temperate lakes, however, the development of stable stratification inhibits the direct downward transfer of surface stresses. In this stratified regime, the dominant motions induced by the wind are internal seiches (Mortimer 1974; Munnich et al. 1992). These oscillatory motions are now considered to be the principal sources of stirring in the lake interior and in the bottom boundary layer (BBL) and thus exert a major control on the availability of nutrients and hence on the growth of phytoplankton (Ostrovsky et al. 1996).

Observations of internal seiche motions in lakes have, until relatively recently, been restricted to data from one or more strings of temperature recorders (Frempong 1983). The horizontal velocities associated with seiches in most basins are weak, typically exhibiting a root mean square (rms) value of a few cm s$^{-1}$ and are, therefore, too small to be measured with rotor or propeller current meters. In the last two decades, however, it has become possible to resolve these small motions using Acoustic Doppler Current Profilers (ADCPs). Taking advantage of the long time scale of internal seiches (typically hours), noise levels can be reduced to $\sim$ 1 mm s$^{-1}$ by averaging velocity measurements over periods of several minutes or more. This ability of ADCPs to measure seiche velocities directly has been used to elucidate the modal structure of internal seiches (Antenucci et al. 2000; Lorke and Wuest 2005; Simpson et al. 2006).

Acoustic Doppler instruments can also be used to determine the rate of turbulent energy dissipation, $\varepsilon$, which is a key determinant of vertical mixing. In marine systems, velocity differences along the acoustic beams of an ADCP have been used to generate a structure function (SF) from which $\varepsilon$ can be derived (Wiles et al. 2006). To apply this

*Correspondence: j.h.simpson@bangor.ac.uk

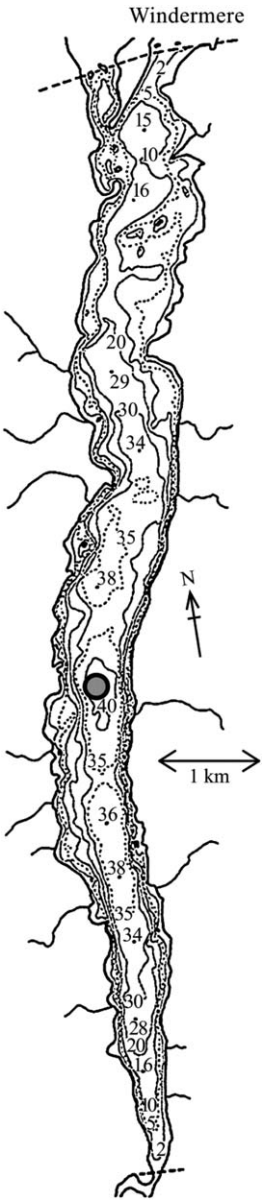


**Fig. 1.** Windermere South Basin bathymetry (m; after Ramsbottom 1976). The filled circle shows the position of the ADCP and temperature chain moorings. Windspeed and direction were recorded on an adjacent buoy with sensors at a height of 2.3 m.

approach to lakes, where energy levels are generally low, it is necessary to use an ADCP operating in pulse-pulse (p-p) coherent mode which furnishes low-noise velocity estimates at the cost of a compromise in acoustic range, which is limited to a few meters. Measurements of this kind, made from bed-mounted ADCPs in the BBL of lakes, have shown that the predominant stirring mechanism in the boundary layer is the motion induced by internal seiches (Lorke et al. 2003, Simpson et al. 2011).

In this contribution, we report a further development in which measurements of the dissipation rate $\varepsilon$, via the SF approach, have been made in both the BBL and in the interior of the water column in parallel with full water-column measurements of flow and temperature structure. The observations commenced in the mixed winter regime and continued during the onset of surface heating and the development of the stratified summer regime so that we have been able to observe the changes in flow and mixing during the transition to a stable water column.

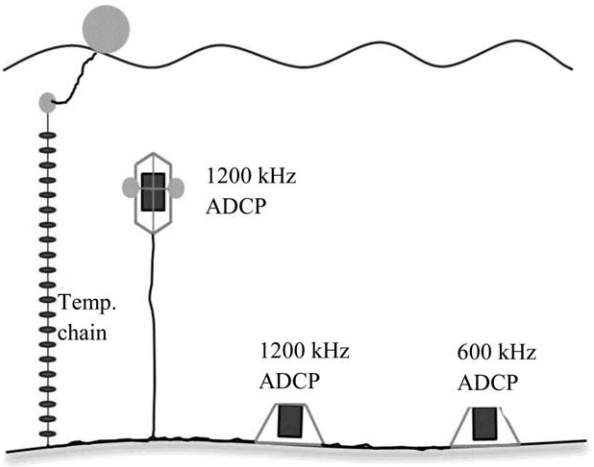


**Fig. 2.** Mooring configuration for all deployments. The instruments were located along the axis of the lake with the temperature chain and the 600 kHz ADCP separated by $\sim$ 85 m from the centrally positioned 1200 kHz bed-mounted ADCP. The tethered ADCP was located at $\sim$ 30 mab (depth approximately ten meters) for deployment 1 and at 25 mab (depth $\sim$ 15 m) for deployments 2 and 3. The uppermost temperature logger was located at 37 mab, i.e., approximately three meters below the water surface. The full water column depth was 40.5 $\pm$ 0.4 m.

## *Methods*

### Windermere observations

Windermere is the largest natural lake in England and one of the best studied in the world (Talling 1999; Maberly and Elliott 2012). It has been a focus for studies in physical limnology since the pioneering work of Clifford Mortimer who made careful measurements of the changes in water column temperatures and used them to clarify the nature and importance of seiche motions in lakes (Mortimer 1952). The lake is long (16.9 km), narrow and effectively divided into two separate basins by islands and a shallow sill (depth approximately two meters). The observations reported here were made near the center of the longer ($\sim$ 11 km) southern basin (Fig. 1) which has a maximum depth of 42 m and a width which does not exceed one kilometer.

A combination of three ADCPs and a temperature chain were deployed in the configuration shown in Fig. 2 starting on 10 April 2013 (day of the year [DOY] 99) when the lake was still vertically well mixed. A single 600 kHz ADCP, operating in mode 12 (multiple subpings) with bin size set to $\Delta z = 1$ m, was used to measure flow in the water column

from 2.6 m above bed (mab) to within approximately three meters of the surface in a water column of depth 40.5 ± 0.4 m. Velocity profile data were recorded at intervals of $\Delta t = 60$ s, based on 50 subpings. The developing thermal structure of the lake was measured, at intervals of $\Delta t = 60$ s, by an adjacent chain of temperature microloggers with sensors spaced at intervals of $\Delta z = 1.5$ m above 30 m depth and $\Delta z = 3.5$ m below. The uppermost temperature logger was located at 37 mab, that is, approximately three meters below the water surface.

For the turbulence observations, two 1200 kHz ADCP units were employed, one mounted on a heavy frame on the lake bed and a second on a buoyant float attached to a bottom anchor by a taught line (Fig. 2). Both these instruments operated in pulse-pulse coherent mode 5, in which the Doppler shift is found from the relative phase of two consecutive coherent pulses. The bin size was initially set to $\Delta z = 5$ cm with an ambiguity velocity setting of $v_a = 5$ cm s$^{-1}$. To avoid phase wrap-around, the available range $R_m$ was restricted to:

$$R_m = \frac{c^2}{8 v_a f_0} \tag{1}$$

(Lhermitte and Serafin 1984), where $c$ is the velocity of sound in water and $f_0$ is the operating frequency of the ADCP, which implies $R_m \approx 4$ m. Data based on the average of two subpings were recorded at intervals of one second which allowed a continuous recording time of ∼ 14 d with an rms velocity uncertainty of 0.43 cm s$^{-1}$. For deployments 2 and 3, the bin size was modified to $\Delta z = 8$ cm with single pings recorded at intervals of one second giving an rms velocity uncertainty of 0.49 cm s$^{-1}$. For the final deployment (3), data sampling was changed from continuous recording to a 50 : 50 duty cycle (300 s recording : 300 s off) which permitted the acquisition of a 27 d record. The tethered ADCP was located at ∼ 30 mab (depth approximately ten meters) for deployment 1 and at 25 mab (depth ∼ 15 m) for deployments 2 and 3.

Wind speed and direction were recorded at a height of 2.3 m above the lake surface by a meteorological station located on a buoy close to the ADCP moorings. The meteorological station also provided measurements of the downward flux of solar radiation at the lake surface and was equipped with a second temperature chain which furnished additional temperature profile data, recorded at intervals of $\Delta t = 240$ s.

**Internal seiche analysis**

The periods and modal structure of the internal seiche motions were determined by cross-spectral analysis of the ADCP time series using standard analysis techniques (Emery and Thomson 1998). The cross-spectra between the along-lake velocity at each level and that at the lowest bin level were used to determine the co- and quadrature spectra at each frequency and hence, the modal structure (amplitude, phase, and coherence) of the seiche motions. Forming the cross-spectrum (*Pxy*) of the velocity at each level with the near-bed flow has the advantage of improving the signal-to-noise ratio since the flow close to the bed tends to be dominated by seiche motions and is relatively free from "noise" associated with less regular motions further up the water column (Simpson et al. 2011).

The vertical density structure of the lake controls the phase speed and modal structure of seiche motions. To determine the theoretical form of the modes, the vertical density gradient, derived from the temperature profile data, was used to obtain the profile of $N^2$ the square of the buoyancy frequency which is defined as:

$$N^2 = -\frac{g}{\rho}\frac{\partial \rho}{\partial z} \tag{2}$$

where $g$ is the acceleration due to gravity and $\rho(z)$ is the density. The modal structure and phase speed of each mode can be obtained from $N^2(z)$ using standard internal wave theory (Gill 1982) in a numerical code (Klink 1999).

**Measures of kinetic energy and stratification**

The velocity time series from the 600 kHz ADCP was used to determine the depth-average velocity component (strictly an average over the 86% of the water column covered by the ADCP profiles) which was subtracted from the full profile to yield the depth varying component. From these two velocity components, the depth-uniform (barotropic) and depth-varying (baroclinic) kinetic energies (KE, J m$^{-3}$) were obtained.

As a measure of the strength of water column stratification, we use the potential energy anomaly $\phi$ (Simpson 1981) which is determined from the density profile according to:

$$\phi = \frac{1}{h}\int_{-h}^{0} (\bar{\rho} - \rho(z)) g z dz; \;\; \bar{\rho} = \frac{1}{h}\int_{-h}^{0} \rho(z) dz \tag{3}$$

where $h$ is the depth of the water column. $\phi$ is the amount of energy per unit volume required to completely mix the water column. It is zero in fully mixed conditions and increases with stratification.

**Dissipation via the Structure function**

In the Structure Function Method (Wiles et al. 2006), the raw along-beam velocity components $v(z)$ from each beam are used to estimate a second order SF which is defined as:

$$D(z,r) = \overline{(v'(z) - v'(z+r))^2} \tag{4}$$

where $v' = v(z) - \bar{v}(z)$ is the fluctuating component of velocity at position $z$ along the beam. $D(z,r)$ is the mean-square of the velocity fluctuation difference between two points

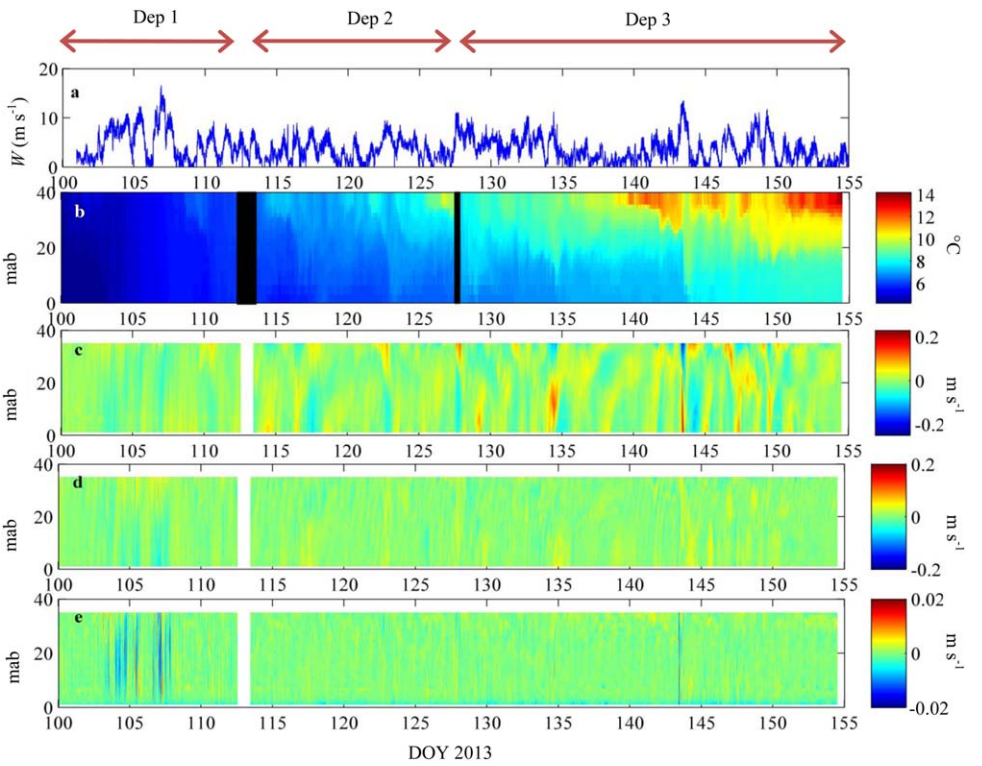


**Fig. 3.** Windspeed, temperature, and velocity. Panels show observations covering all three deployment periods (dep 1–3) for: (a) windspeed $W$ (m $s^{-1}$) at 2.3 m height above the lake surface; (b) Water column temperature (°C); (c) axial velocity component (m $s^{-1}$); (d) transverse velocity component (m $s^{-1}$); (e) vertical velocity component (m $s^{-1}$), note change of scale.

separated by a distance $r$. For isotropic turbulence, the SF $D(z,r)$ is related to the dissipation $\varepsilon$ by:

$$D(z,r) = C_v^2 \varepsilon^{2/3} r^{2/3} \tag{5}$$

where $C_v$ is a constant taken to have a value of 1.45. For a given $\varepsilon$, $D$ should increase as $r^{2/3}$ from $D = 0$ at $r = 0$. In practice, $D \to M$ as $r \to 0$ where $M = 2\sigma_v^2$ is twice the variance of velocity estimates at a point due to instrumental noise of the ADCP. The observed $D(z,r)$ is therefore fitted to an equation of the form:

$$D(z,r) = M + Ar^{2/3} \tag{6}$$

to estimate $M$ and the dissipation $\varepsilon$ from $A$ according to:

$$\varepsilon = \frac{A^{3/2}}{C_v^3} \tag{7}$$

Dissipation values derived from the SF from four beams, which may differ according to orientation relative to shear stress in the flow (Wiles et al. 2006), are averaged to provide a best estimate of $\varepsilon$ at each level.

Whereas previous ADCP measurements of $\varepsilon$ in lakes have utilised instruments fixed on a frame sitting on the lake bed, the observations reported here also include data from an ADCP mounted on a buoyant float in mid-water. This mode of operation on a tethered buoy has recently been validated by comparison with a Vertical Microstructure Profiler (VMP) shear probe measurements (Lucas et al. 2014) which demonstrated that the motions of the tethered buoy do not compromise the estimation of $\varepsilon$ because the SF method is based on velocity differences which are not significantly affected by buoy motion. These measurements also confirmed the validity of the constant $C_v = 1.45$, originally determined from Doppler radar measurements of turbulence in the atmosphere (Sauvageot 1992), for dissipation measurements in water.

The SF $D(z,r)$ was constructed for each acoustic bin of each beam from differences of the fluctuating velocity component $v' = v(z) - \bar{v}(z)$ over a range of separations of up to 1.35 m. The temporal mean velocity $\bar{v}(z)$ and the mean square velocity differences were averaged over a period of 300 s to yield $D(z,r)$ from which the dissipation estimates were derived by fitting Eq. 6.

## Results

### The evolution of stratification, flow, and wind forcing

The development of stratification and the corresponding changes in the flow field over the 55 d observation period are illustrated, along with the wind forcing, in the summary plot of Fig. 3. Co-ordinates for the horizontal velocities have

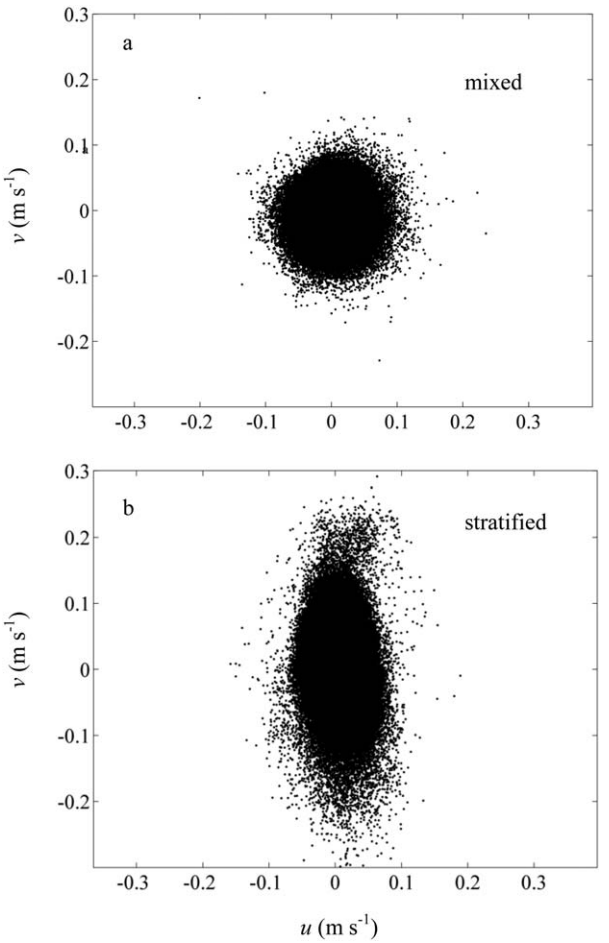


**Fig. 4.** Scatter diagram of horizontal velocity vectors (*u*: transverse and *v*: axial). Data shown for (a) vertically mixed conditions in deployment 1 and (b) for stratified conditions during deployments 2 and 3.

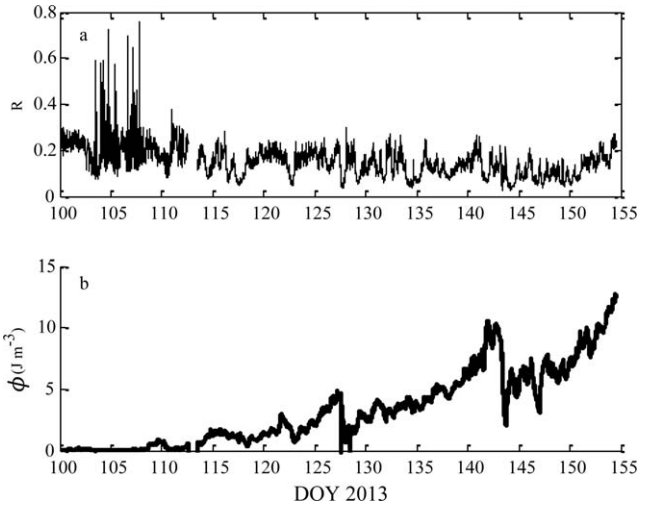


**Fig. 5.** Relative magnitude of vertical motion as stratification develops. Data shown for (a) the ratio $R$ of the vertical and axial flow speeds and (b) the potential energy anomaly $\phi$ (J m$^{-3}$) indicating the development of stratification. ($\phi$ is the amount of energy required to completely mix the water column. It is zero in fully mixed conditions and increases with stratification).

been rotated by 9° so that the components are now along axis $v$ (Fig. 3c) and transverse $u$ (Fig. 3d). Complete vertical mixing of the water column is evident at the start (DOY 100) and prevailed practically to the end of the first deployment (DOY 113) when the strong winds diminished and the onset of some weak stratification becomes apparent. In the mixed regime, the strongest wind episodes (up to 15 m s$^{-1}$) induced axial and transverse currents with speeds at times exceeding $\sim$ 0.05 m s$^{-1}$ in the horizontal and $\sim$ 0.02 m s$^{-1}$ in the vertical.

During the second deployment period, DOY 114–128, surface heating promoted stratification of the water column with the surface to bottom temperature difference reaching $\Delta T \sim 3$°C by the end of the deployment. At the same time, the flow field changed in character as the increasing stratification restricted the direct downward penetration of motion forced by the wind at the surface and inhibited vertical motion to speeds generally less than 0.01 m s$^{-1}$. As stratification was established in deployment 2, baroclinic, periodic flow, with surface and bottom currents in antiphase, developed. This motion, which is characteristic of internal seiche activity, became more pronounced during the third deployment as the water column stability increased.

The change in the flow regime is clearly manifest in the distribution of velocities: during the mixed regime (deployment 1); the scatter diagram of the horizontal velocities (Fig. 4a) exhibits a circular pattern with equal flow speeds along ($v$) and across ($u$) the lake. By contrast, with the onset of internal seiche activity (deployments 2 and 3), the pattern of the velocity distribution (Fig. 4b) becomes roughly elliptical with an axis ratio $\sim$ 2.5 and a marked increase in the magnitude of the velocities although the wind forcing had not increased. At the same time, the development of stratification acts to inhibit vertical motions as is evident from the plot of ratio R of magnitudes of the vertical ($w$) and axial horizontal velocity ($v$) in Fig. 5a. During the mixed regime, this ratio reached values of R $\sim$ 0.7 at times of strong wind forcing. As stratification developed, indicated by the potential energy anomaly $\phi$ (Simpson 1981) in Fig. 5b, R fell to mean values of $\sim$ 0.15 at the end of the observation period.

In both mixed and stratified regimes, the vertically averaged axial velocity had an rms value of $\sim$ 0.011 m s$^{-1}$ which included only a small contribution from the external seiche with an amplitude of $\sim$ 0.0015 m s$^{-1}$ and a seiche period $T_p$ = 19.7 min which did not vary significantly between mixed and stratified conditions.

**Dissipation measurements and wind forcing**

Pulse-pulse coherent velocity measurements, from the two 1200 kHz ADCPs, were analysed, via the SF method, to

yield estimates of the rate of energy dissipation in W kg$^{-1}$. An example of the results for the 3.5 m vertical slice from the upper instrument is shown in Fig. 6. The dissipation rate $\varepsilon$ varied over more than four decades with periods of intense dissipation separated by quiescent periods when $\varepsilon$ falls at times to $\sim 3 \times 10^{-10}$ W kg$^{-1}$; a value which was essentially the same for bottom mounted and midwater instruments.

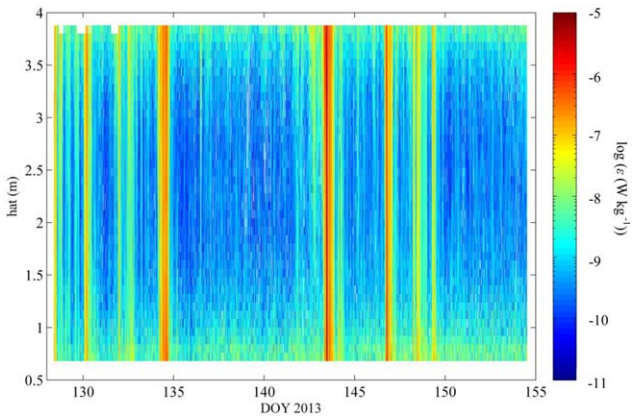


**Fig. 6.** Dissipation $\varepsilon$ from the tethered 1200 KHz ADCP at 25.5 mab (15 m depth). The values of log $\varepsilon$ (W kg$^{-1}$), based on the SF, are plotted vs. height above the transducers, (hat) in meters, for deployment 3.

This background level, which presumably represents the instrument noise, is apparently slightly higher in the bins closest to the ADCP and also in data from bins close to the range limit of approximately four meters. For a best overall estimate of dissipation, the $\varepsilon$ results over the central 1.5–2 m of the profile were averaged. These averaged estimates for both ADCPs are presented in Fig. 7 in parallel with the windspeed $W$, the axial flow and water column stratification for the observation period. The near-bed and midwater $\varepsilon$ results track each other to a considerable degree and both are clearly related to the wind forcing. This relationship is particularly pronounced during the period of the first deployment when the water column was well mixed. In Fig. 8, we show a log plot of the dissipation rate over time at the two levels together with $W^3$.

For homogeneous (uniform density) conditions, we might expect "law of the wall" scaling to apply below the layer influenced by surface waves, so that the dissipation rate would be given by:

$$\varepsilon = \frac{u_*^3}{\kappa z} = \left[\frac{C_d \rho_a}{\rho_w}\right]^{3/2} \frac{W^3}{\kappa z} \tag{8}$$

where $z$ is depth below the surface, $\kappa$ is the von Karman constant, $\rho_a$ , $\rho_w$ are the densities of air and water, respectively,

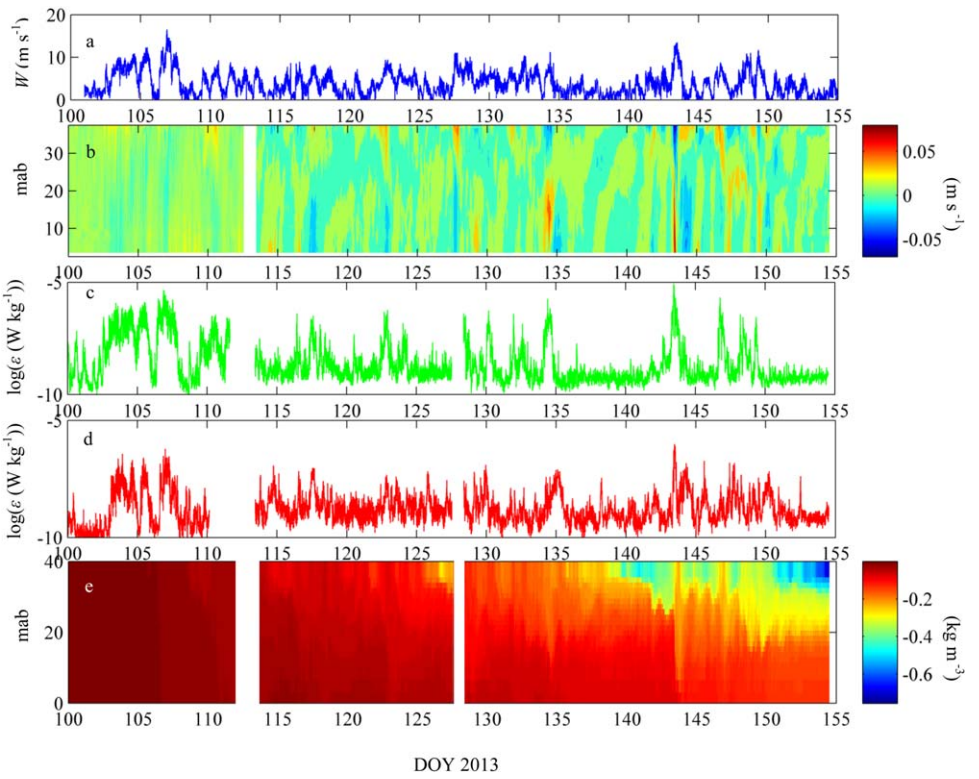


**Fig. 7.** Mean dissipation time series. Data are shown for: (a) Windspeed $W$ (m s$^{-1}$); (b) Axial velocity (m s$^{-1}$); (c) Mean dissipation $\varepsilon$ (W kg$^{-1}$) at 32.1 mab (depth 8.4 m; dep 1) and 28.0 mab (depth 12.5 m; dep 2 and 3); (d) Mean dissipation $\varepsilon$ (W kg$^{-1}$) at 2.1 mab (dep 1) and 2.8 mab (dep 2 and 3); (e) Density anomaly $\Delta\rho$ (kg m$^{-3}$) = density difference from maximum density at 4°C.

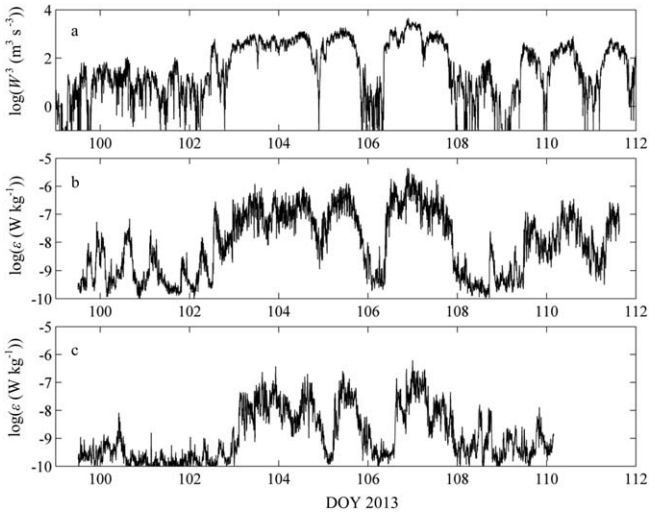


**Fig. 8.** Dissipation in the mixed regime during deployment 1. Data are shown for: (a) $W^3$ (m$^3$ s$^{-3}$); $W$ = windspeed; (b) dissipation $\varepsilon$ at 32.1 mab (depth of 8.4 m); (c) dissipation $\varepsilon$ at 2.1 mab. Values of $\varepsilon$ were averaged over a depth interval of $\Delta z$ = 1.5 m and 300 s in time and $W$ was averaged over 240 s.

and $C_d$ is the drag coefficient. $u_* = \sqrt{\frac{\tau}{\rho}}$ is the friction velocity for the applied wind stress $\tau$ which is assumed to be continuous across the air water interface. This scaling relation may be tested by plotting $\varepsilon$ vs. $W^3$ in log form (Fig. 9a) for the data from the upper level (depth = 8.4 m). The compliance with a slope of unity confirms that the $W^3$ scaling is valid while a linear regression of $\varepsilon$ on $W^3$ gives: $\varepsilon = 3.3 \times 10^{-10}\ W^3 - 7.6 \times 10^{-9}$ with $R^2 = 0.65$ ($t$-test, $t = 34.7$, degrees of freedom [df] = 650, $p = 0.001$). The slope ($3.3 \times 10^{-10}$ m$^{-1}$) is consistent with Eq. 8 for a realistic drag coefficient of $\sim 1.0 \times 10^{-3}$.

By contrast, once the stratified regime is established, this direct relation between dissipation and wind forcing is much diminished as is evident in the log plot of $\varepsilon$ vs. $W^3$ for the period of increasingly robust stability during deployment 3 (Fig. 9b).

### The development of seiche motions

Barotropic and baroclinic KE (J m$^{-3}$) based on the 600 kHz ADCP data and averaged over the water column for six-hour intervals are presented in Fig. 10. While the short-term influence of wind forcing on both baroclinic and barotropic KE levels is apparent over the whole period, there is a significant change in the KE balance between the well mixed regime, seen in deployment 1, and the stable structure which subsequently develops during deployments 2 and 3. In the mixed regime, the barotropic KE is similar to the baroclinic KE for much of the time but towards the end of deployment 1, the two begin to diverge as baroclinic energy increases over time without a significant change in the barotropic energy. Consequently, the total KE increases with

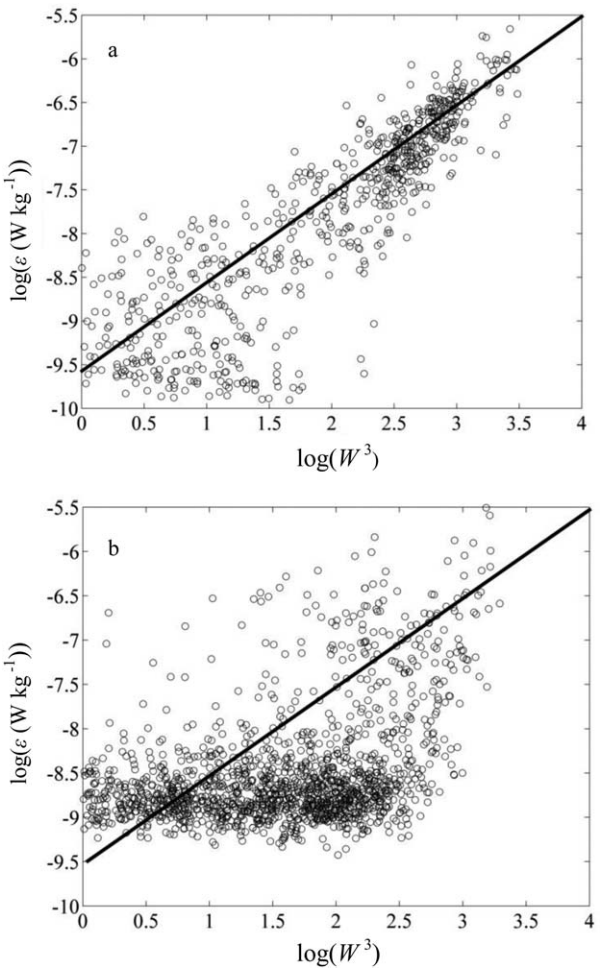


**Fig. 9.** Dissipation vs. $W^3$ as log-log plots for: (a) mixed regime (dep 1): $\varepsilon$ at 32.1 mab (8.4 m depth); (b) Stratified regime (dep 3): $\varepsilon$ at 28.0 mab (12.5 m depth). Both parameters were averaged over 20 min. The straight line in each plot represents a linear dependence of $\varepsilon$ on $W^3$.

time, a surprising result, since the average windspeed does not increase over the observation period.

This change in the KE balance is associated with the development of stratification which commences from DOY 110 and becomes well established by DOY 140 when there is a surface to bottom temperature difference of $\Delta T \sim 4$°C and $\phi \sim 6$ J m$^{-3}$ (Fig. 5b). Long period (2–3 d) motions, with surface and bottom flow in antiphase, are apparent from around DOY 117. By DOY 145, stratification has intensified ($\Delta T > 4$°C) and there are pronounced, shorter period (approximately one day) oscillations evident in the isotherms and in the axial flow. A cross-spectral analysis between the velocity at each bin level and that of the lowest bin for DOY 145–155 (Fig. 11) reveals a dominant first mode oscillation with a broad spectral peak centered on a frequency of 0.0352 c h$^{-1}$ (cycles per hour) and a half power width of $\Delta$f $\sim$ 0.0235 c h$^{-1}$ which corresponds to periods in the range $T_p$ = 21–43 h with a maximum at $T_p$ = 28.4 h.

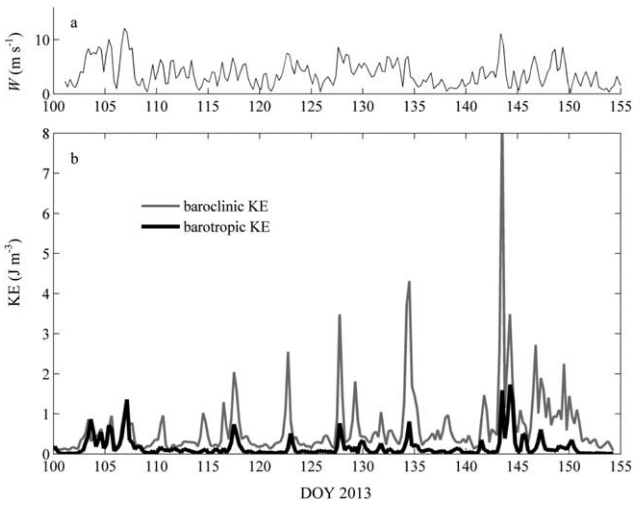


**Fig. 10.** Baroclinic and barotropic kinetic energy. (a) Windspeed $W$ (m $s^{-1}$); (b) barotropic (black) and baroclinic (gray) kinetic energy (J $m^{-3}$) averaged over six hours.

In this frequency band, there is a minimum in the coherence, determined relative to the near-bed velocity, at a height of $\sim$ 22.5 mab with a corresponding change in phase of $\sim$ 180° (Fig. 11b). The energy in this spectral peak accounts for a high proportion (> 60%) of the total kinetic energy in the near bed flow. The phase speed of this lowest mode, calculated from normal mode theory (Gill 1982; Klink 1999) and based on the observed density distribution (Fig. 7e), is $c$ = 0.1305 m $s^{-1}$. This value corresponds to the observed period in a basin of length approximately seven kilometer which is approximately the length of Windermere's southern basin at the level of the 15 m contour.

An estimate of the Rossby radius based on the above value of $c$, and the Coriolis parameter $f = 1.181 \times 10^{-4}$ $s^{-1}$ yields $Ro = c/f$ = 1.105 km which indicates that the seiche motion would have had a significant progressive Kelvin wave component. After subtracting the standing wave component, consisting of two equal and opposite progressive waves, the amplitude of the residual Kelvin wave component at the lake boundaries is $\sim 0.42 \times$ that of the standing wave. Along the center line of the lake, where the moorings are located, the motion would have been dominated by the standing wave component. Earlier in the observation period, when stratification was weaker, the dominant seiche frequency was considerably lower. Spectral analysis for DOY 135–145, for example, shows a dominant first mode oscillation with a peak at a frequency of 0.0178 cycles per hour (c $h^{-1}$) (period $T_p$ $\sim$ 60 h) implying a stronger influence of the Earth's rotation with a considerably larger Kelvin wave component.

### Dissipation in the BBL

The close relation of dissipation in the BBL to wind forcing, which is clearly apparent in the deployment 1 period

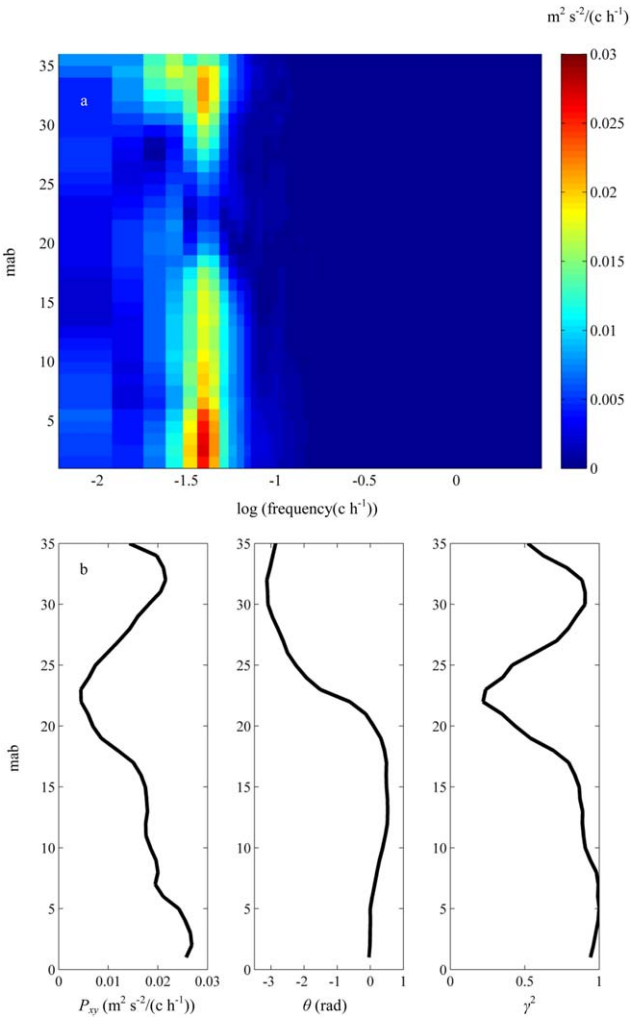


**Fig. 11.** Axial velocity cross-spectrum for DOY 145.1–155.5, 2013. Plots shown are: (a) the amplitude of the cross-spectral power density $Pxy$ ($m^2$ $s^{-2}$/[c $h^{-1}$]) between the axial velocity at each level and the near bed velocity (b) three profiles, vs. height above bed, of $Pxy$, the relative phase angle $\theta$ (radians) and $\gamma^2$ (coherency squared), all at the dominant frequency. $Pxy = (Co^2 + Qu^2)^{1/2}$ where $Co$ and $Qu$ are the in-phase and quadrature components of the cross-spectrum.

(Figs. 8, 9), diminishes substantially with the onset of stratification as the internal seiche motions become the dominant source of turbulence. In the stratified regime, observed during deployment 3, dissipation in the BBL is seen to be closely related to the oscillatory axial flow in the seiche motions. A comparison of the dissipation from the SF at 2.5 m above the bed and the axial flow velocity $v$ and the cube of the speed $|v|^3$, all parameters being averaged over ten minutes (Fig. 12) shows a clear visual correlation of $\varepsilon$ with $|v|^3$. When the two parameters are plotted against each other in log-log form (Fig. 12d), there is considerable scatter but at higher flow rates ($|v| > 2$ $cm^{-1}$), the data lie around a line of unity slope, indicating proportionality of $\varepsilon$ and $|v|^3$ and, hence, suggesting conformity with the "law of the wall."

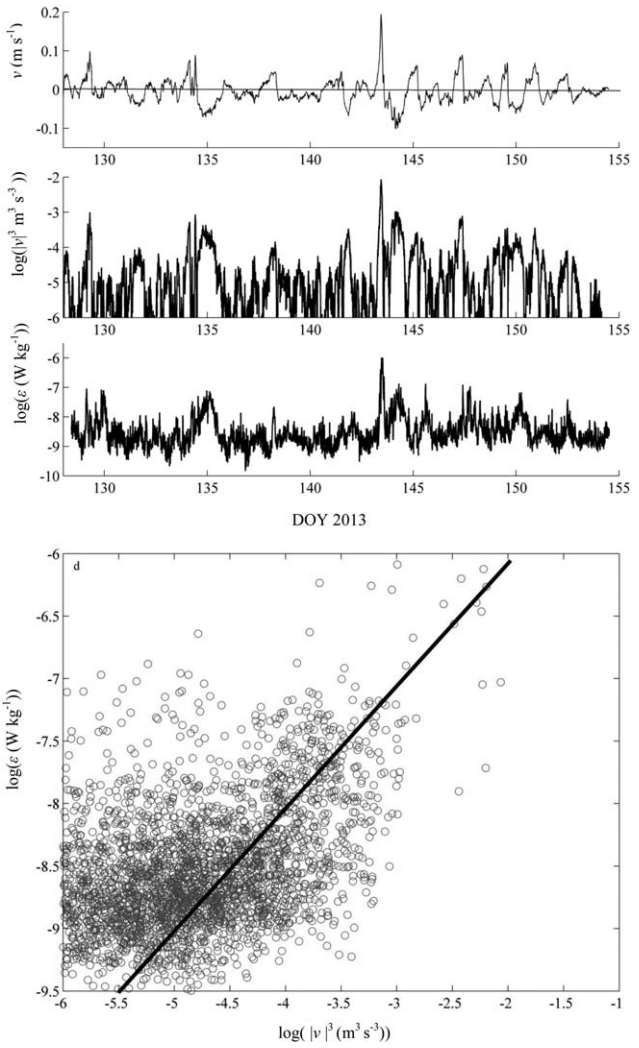


**Fig. 12.** Dissipation vs. $|v|^3$ in the BBL during deployment 3 (stratified regime). (a) Near-bed axial velocity $v$ (m s$^{-1}$); (b) cube of near-bed flow speed $|v|^3$ (m$^3$ s$^{-3}$); (c) $\varepsilon$ (W kg$^{-1}$) at 2.8 mab; (d) log $\varepsilon$ (W kg$^{-1}$) vs. log $|v|^3$ (m$^3$ s$^{-3}$). The straight line with a slope of unity would indicate a linear relation between the variables.

The intercept of $\sim -4$ on the log-log plot indicates a bottom drag coefficient of $\sim 2.0 \times 10^{-3}$ which is consistent with accepted values for this parameter in lakes (Wuest and Lorke 2003).

### Dissipation and heat flux in the pycnocline

Following the onset of stratification, energy dissipation in the pycnocline region becomes highly intermittent in character as is evident in Fig. 13 which shows the average $\varepsilon$ between 11.5 m and 13.5 m depth in parallel with the axial velocity shear $(\partial v/\partial z)^2$, based on differences over 2 m and the stability frequency as $N^2$ from differences over 1.5 m. Periods of several days, during which very low dissipation ($\sim 10^{-9}$ W kg$^{-1}$) prevails, are separated by energetic episodes in which $\varepsilon$ increased by up to three orders of magnitude for

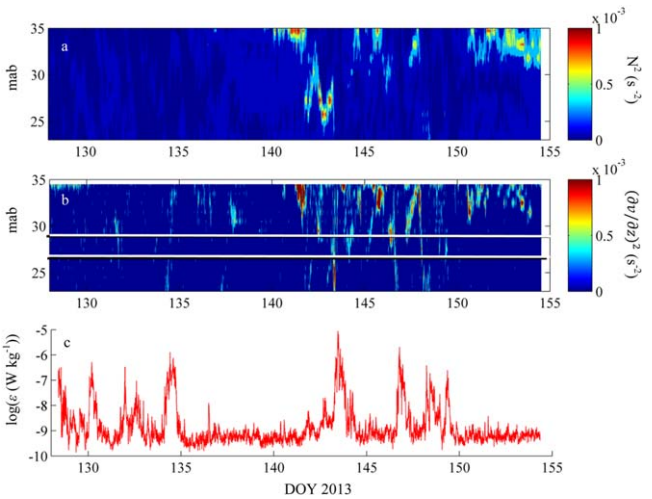


**Fig. 13.** Mixing in the pycnocline during deployment 3 (stratified regime): (a) $N^2$ (s$^{-2}$), buoyancy frequency squared based on differences over 1.5 m from temperature chain data. (b) Velocity shear squared $(\partial v/\partial z)^2$ (s$^{-2}$) based on differences over 2 m; (c) Average dissipation $\varepsilon$ (W kg$^{-1}$) in the interval between 27.0 mab and 29 mab (11.5 m and 13.5 m depth) which is indicated in (b) by the white horizontal lines.

approximately one day (Fig. 13c). These high dissipation pulses are clearly related to maxima in the axial velocity shear from the 600 kHz ADCP measurements at the same level (Fig. 13b). The distribution of shear over depth and time exhibits a similar pattern to that of $N^2$ (Fig. 13a) but efforts to relate the observed dissipation rates to the relevant gradient Richardson numbers were unsuccessful probably because of the difficulty of achieving accurate spatial matching of the shear and $N^2$ measurements which were based on sensors separated horizontally by $\sim$ 170 m.

The downward flux of heat due to internal mixing may be estimated directly from $\varepsilon$ by using the Osborn relation for the vertical diffusivity $K_z$:

$$K_z = \frac{\Gamma \quad \varepsilon}{N^2} = \frac{\Gamma \quad \varepsilon}{g\alpha\partial T/\partial z} \tag{9}$$

where $\alpha$ is the expansion coefficient, $N$ is the buoyancy frequency, and $\Gamma \sim 0.2$ is the mixing efficiency. The diffusive downward flux of heat is then just:

$$Q_d = -c_p \rho K_z \frac{\partial T}{\partial z} = \frac{c_p \rho \Gamma}{g\alpha} \varepsilon (Wm^{-2}) \tag{10}$$

This heat flux, acting over a time interval of $\Delta t$, would increase the mean temperature of the water column of average depth $h_b$ below the ADCP by:

$$\Delta \bar{T} = \frac{\Gamma \bar{\varepsilon}}{g\alpha h_b} \Delta t \tag{11}$$

A component of solar radiation $q_s(z)$ may also be transmitted directly downwards through the water column to

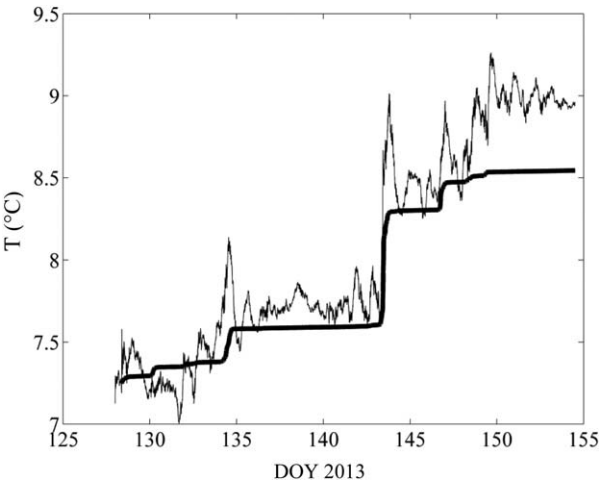


**Fig. 14.** Heat flux and water column heat content. The fine line shows the average temperature of the water column below the ADCP which was measuring dissipation during deployment 3. The thick line represents the temperature rise resulting from the pycnocline heat flux based on the observed dissipation.

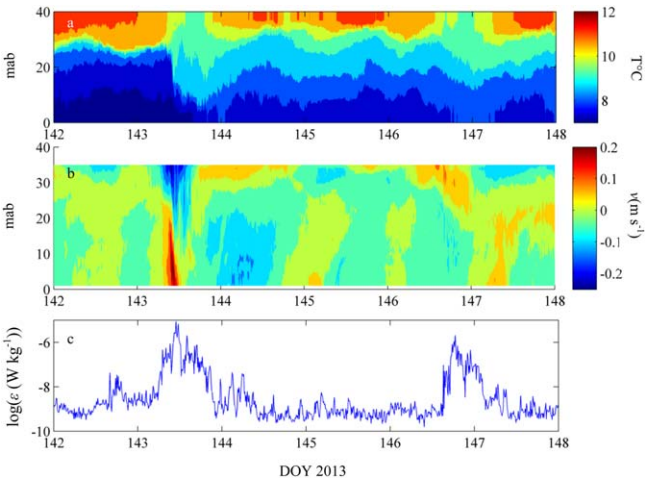


**Fig. 15.** Strong mixing event between DOY 142 and 148. (a) Temperature time-depth contours; (b) axial velocity $v$ (m s$^{-1}$); (c) dissipation $\varepsilon$ (W kg$^{-1}$).

supplement the diffusive heat flux (Jassby and Powell 1975). An estimate of this contribution based on observations of the average solar radiation (193 W m$^{-2}$) at the lake surface and the diffuse attenuation coefficient in the surface waters ($K_d \sim 0.5$ m$^{-1}$) indicates that, in this case $q_s(z)$ is small ($< 1$ W m$^{-2}$).

During deployment 3, the mean dissipation at 12.5 m depth was $\bar{\varepsilon} = 2.87 \times 10^{-8}$ W kg$^{-1}$ which, on the basis of Eq. 10, implies an average heat flux of $Q = 30.4$ W m$^{-2}$ over the 27.5 d period of deployment. To determine $h_b$, the height of the water column below the $\varepsilon$ measurements, we have generated a new hypsometry derived from a recent multibeam survey of Windermere (Miller et al. 2013). Applying the diffusive flux to the underlying water for $h_b = 16.9$ m and $\Delta t = 26.1$ d, the temperature rise would be $\Delta\bar{T} \sim 1.29$°C. The time course of $\Delta\bar{T}(t)$ based on Eq. 11 and the time integral of $\varepsilon$ is compared in Fig. 14 with the actual temperature increase in the water below 12.5 m depth determined from the temperature chain observations. Abrupt changes in temperature, notably at DOY 134, 143, and 147, coincide in the two records with episodes of high dissipation. The overall temperature rise based on the diffusive flux ($\sim 1.29$°C) is, however, markedly less than that indicated by the observed temperature profiles ($\sim 1.75$°C), which implies that not all mixing is represented in observations in the middle of the lake basin.

The most energetic mixing event during deployment 3 was that which occurred on DOY 143 (Fig. 15) when the wind reached 13 m s$^{-1}$ and induced a strong first mode response with flow speeds exceeding 0.2 m s$^{-1}$ in the near surface and near bed flows. Dissipation reached peak values of $10^{-5}$ W kg$^{-1}$ and remained higher than background levels for approximately one day during which there was a dramatic change in the temperature structure with large movements of the isotherms and an irreversible change of approximately $-0.8$°C in the average temperature of the water below 15 m depth.

## Discussion

We have observed changes in water column structure, flow and the rate of turbulent energy dissipation $\varepsilon$ in a temperate lake during the transition between vertically mixed and stratified regimes which follows the onset of surface heating in spring. Measurements of $\varepsilon$ have been achieved by applying the SF analysis to velocity data from two pulse-pulse coherent Doppler profilers, one located on the lake bed and the other deployed in the upper part of the water column on a tethered float.

In the initial, well-mixed regime (DOY 99–113), the wind-driven motions exhibited comparable barotropic and baroclinic flows with along-axis and transverse components of practically the same magnitude. The strongest wind episodes (up to 15 m s$^{-1}$) induced flows with speeds, at times, exceeding $\sim 0.05$ m s$^{-1}$ in the horizontal and $\sim 0.02$ m s$^{-1}$ in the vertical. There was a strong correlation between dissipation and the wind forcing represented by the cube of the wind-speed $|W|^3$. This relationship, which was especially clear at the level of the upper ADCP measurement (depth 8.4 m), is consistent with 'law of the wall' scaling for $\varepsilon$.

When surface heating started to promote stratification of the water column (DOY 114 onward), the character of the flow was radically changed through the development of the baroclinic periodic motions associated with internal seiches which became increasingly prevalent in the latter part of the observational period. With the onset of internal seiches,

there came a marked change in the scatter diagram of flow velocities which was transformed from circular to elliptical form with axial speeds greater by a factor of $\sim 2.5$ than those of transverse flow. Stratification was also observed to suppress vertical motions; the ratio of vertical to horizontal flow speeds was reduced from peaks of $\sim 0.7$ in the mixed regime to $\sim 0.1$ in the stably stratified system.

The seiche motions are dominated by a mode 1 wave with a decreasing period which was $\sim 25$ h during the last ten days of the recording period (DOY 145–155). Even at this time, when stratification was well established, estimates of the Rossby radius indicated the influence of the Earth's rotation on the motions which involved a significant progressive Kelvin wave component at the boundaries of the lake.

The stirring effects of the seiche motions are apparent in both the BBL and in the pycnocline. In the BBL, most of the dissipation occurred in a number of strong maxima (approximately two decades above background) which were found to coincide with peaks of the near-bed flow speed in the seiche motions. Dissipation here was found to exhibit a correlation with $|v|^3$ indicating law of the wall scaling.

In the pycnocline (12.5 m depth), $\varepsilon$ was close to the noise level ($\sim 3 \times 10^{-10}$ W kg$^{-1}$) for much of the time but exhibited pronounced maxima (approximately three decades above background) which are clearly related to maxima in the square of the axial velocity shear $(\partial v/\partial z)^2$. These episodes of strong mixing involve peak $\varepsilon$ values which are significantly larger than the dissipation maxima in the BBL although, because $N^2$ values in the pycnocline are larger by almost an order of magnitude, vertical mixing rates are generally lower than in the BBL. During deployment 3, average dissipation in the pynocline exceeded that in the BBL by a factor of approximately three while the mean $N^2$ was greater by a factor of approximately six than in the BBL which indicates that the average $K_z$ in the BBL was greater than that in the pycnocline by a factor of approximately two.

The spatial mismatch of $\varepsilon$ and $N^2$ (separation $\sim 80$ m) is less severe than that for shear and $N^2$ and may be used to make provisional rough estimates of the diffusivity and the Ozmidov length scale in the pycnocline during deployment 3. Values of the diffusivity $K_z$ based on Eq. 9 range from $\sim 3 \times 10^{-6}$ m$^2$ s$^{-1}$ to $3 \times 10^{-3}$ m$^2$ s$^{-1}$ with a mean of $\sim 8 \times 10^{-5}$ m$^2$ s$^{-1}$. Estimates of the corresponding values of the Ozmidov length $L_O = \sqrt{\frac{\varepsilon}{N^3}}$ in the pycnocline ranged from a few centimeters in quiescent periods to approximately five meters in energetic episodes, with a mean value of 0.21 m. This value is only a few times the bin separation, so the requirement for $L_O$ to exceed the scale at which the turbulence is sampled (Wiles et al. 2006), may seem to be compromised. $L_O$, however, increases with $\varepsilon^{1/2}$ so that, at times of significant dissipation, our sampling interval of 5–8 cm should have been adequate. The convincing fits of SF to the $r^{2/3}$ form shown in Lucas et al. (2014) support this inference.

The high levels of ε occurring in the pycnocline indicate that, in Windermere, significant energy transformation from large to small scales is occurring in the pycnocline as well as in the BBL a result which bears on the question of where vertical mixing is occurring (Wuest and Lorke 2003). Integration of $\varepsilon$ in the pycnocline over a 26.1-d period provided an estimate of the downward diffusive heat flux (average $\sim 30$ W m$^{-2}$) which accounted for $\sim 73\%$ of the temperature rise in the water column below. Abrupt increases in the heat content of the lower layers follow the pattern of intense, relatively brief, episodes of dissipation in the pycnocline. The fact that the temperature of the hypolimnion rose considerably faster than can be accounted for by the downward heat flux due to mixing in the thermocline, provides support for the proposal (Thorpe 1998; Gloor et al. 2000; Wuest and Lorke 2003) that some substantial component of internal mixing occurs at the margins of the lake where the pycnocline is in contact with the lake bed. Our conclusion here, however, should be regarded as provisional in view of some uncertainty in the comparison of heat flux and temperature rise, mainly due to the spread of values for the mixing efficiency $\Gamma$ (Thorpe 2005). The choice of $\Gamma \sim 0.2$, although widely used, is at the top end of proposed values for this parameter (Shih et al. 2005) so that our estimate of the fraction of vertical mixing occurring in the interior of the lake should be regarded as an upper bound, i.e., at least 27% of the mixing is not accounted for by our $\varepsilon$ measurements in the center of the lake. While the potential importance of enhanced mixing at the margins of lakes and its dependence on bathymetric slope at the margins have been widely canvassed (Imberger 1998; Boegman et al. 2005; Bouffard et al. 2012), there is a paucity of quantitative estimates of the magnitude of its contribution. There is, therefore, considerable scope for further measurements of the heat flux based on time series of $\varepsilon$ in a variety of lake environments to determine the extent of boundary mixing and its dependence on bottom slope around the margins of a lake.

An interesting and, perhaps, surprising result of our observations is that the total kinetic energy in the lake increases by a factor of approximately three between deployments 1 and 3 as stratification becomes established. This increase occurs in spite of the fact that the winds were generally weaker in the latter part of the observation period. The change in KE may result from more efficient energy input from the wind due to near resonance between the first mode oscillation and the diurnal component of the wind which is evident in Fig. 10a. Alternatively, it may be due to less effective energy dissipation in the stratified regime requiring higher KE levels. If energy input had increased, we would expect to see enhanced dissipation either in the BBL or the pycnocline or both. The time course of wind-stress KE and dissipation (Fig. 16) shows that the rise in total KE was not accompanied by an increase in the rates of dissipation in the BBL or pycnocline. The implication is that, once the lake is stratified, higher KE levels are required to sustain sufficient average dissipation to match the mean input from the wind.

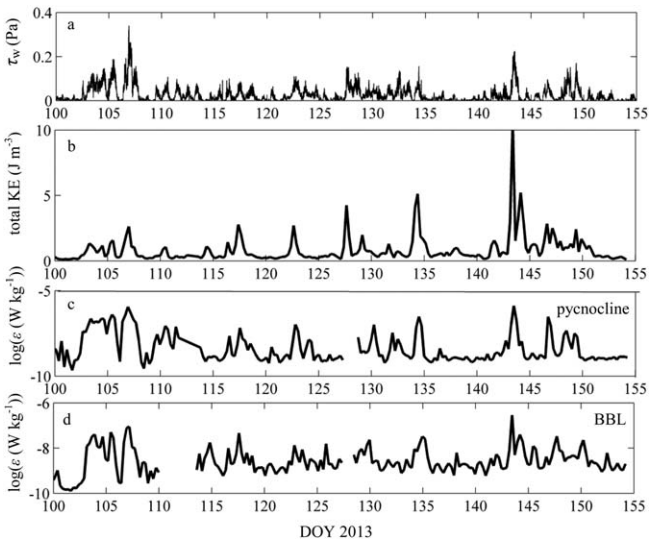


**Fig. 16.** Total kinetic energy and dissipation in mixed (dep 1) and stratified (dep 3) regimes: (a) wind-stress (Pa); (b) total water column KE (J $m^{-3}$); (c) pycnocline dissipation $\varepsilon$ (W $kg^{-1}$); (d) BBL dissipation $\varepsilon$ (W $kg^{-1}$).

In the stratified regime where the damping of large scale motion is considered to be mainly due to BBL dissipation, the time scale $\tau$ for KE decay may be estimated from the decay time $\tau = \frac{\overline{h\mathrm{KE}}}{\bar{\varepsilon}}$ where $\overline{\mathrm{KE}}$ (J $m^{-3}$) is the average total KE, $h$ is the water column depth, and $\bar{\varepsilon}$ (W $m^{-2}$) is the average total dissipation in the BBL. This leads to an estimate of $\sim$ 36 h for the stratified condition of deployment 3. The corresponding figure for KE decay by BBL dissipation during deployment 1 is $\tau \sim 21$ h which supports the conclusion that weaker damping in the stratified regime is responsible for the increase of total water column kinetic energy from the level observed in the mixed water column.

The average rate of dissipation in the BBL in the stratified regime (deployment 3) was $1.6 \times 10^{-4}$ W $m^{-2}$ which is very similar to an estimate of BBL dissipation for Lake Alpnach $1.5 \times 10^{-4}$ W $m^{-2}$ estimated from an extended series of temperature microstructure profiler measurements (Wuest et al. 2000). These authors used their measurements to estimate the KE budget and the levels of dissipation in the epilimnion and hypolimnion of the lake. Such energy balance studies should be enhanced, in future, by continuous time series observations of flow and dissipation of the kind we have obtained in Windermere. Measurements with tethered instruments at several levels will avoid the constraints of the labor intensive procedures and limited sampling which are inherent in microstructure profiling.

The heat flux comparison indicates that useful estimates of vertical diffusivity ($K_z$) can be obtained via the Osborn relation from mid water observations of $\varepsilon$ and $N^2$, provided both are measured at closely adjacent positions; with hindsight a weakness of our observations was the relatively large separation of the temperature chain and ADCP measurements, a separation which should clearly be minimised in future observations. The more general limitation of the ADCP approach, described here, to the measurement of dissipation and diffusivity lies in the range restriction imposed on pulse-pulse operation by phase wrapping which means that a number of p-p Doppler instruments will be necessary to give a full picture of mixing through the water column.

As well as providing a new and more detailed picture of flow and mixing processes during the seasonal transition of a lake from mixed to stratified conditions, the results reported here indicate the potential of midwater observations with p-p coherent ADCPs for studies of internal mixing in lakes. Both the close conformity of the temperature rise in the hypolimnion to bouts of high dissipation in the pycnocline and the observation of "law of the wall" dissipation in the mixed regime support the conclusion of Lucas et al. (2014) that velocity data from instruments mounted on tethered buoys can yield valid estimates of dissipation via the Structure Function method and thus allow long-term measurements of mixing in the water column with dissipation noise levels $\sim 3 \times 10^{-10}$ W $kg^{-1}$, a level comparable to those achieved with the best shear probes. By combining continuous measurements of $K_z$ with gradients of biogeochemical parameters, it should be possible to achieve estimates of the corresponding fluxes.

## References

Antenucci, J. P., J. Imberger, and A. Saggio. 2000. Seasonal evolution of the basin-scale internal wave field in a large stratified lake. Limnol. Oceanogr. **45**: 1621–1638. doi:10.4319/lo.2000.45.7.1621

Boegman, L., G. N. Ivey, and J. Imberger. 2005. The degeneration of internal waves in lakes with sloping topography. Limnol. Oceanogr. **50**: 1620–1637. doi:10.4319/lo.2005.50.5.1620

Bouffard, D., L. Boegman, and Y. R. Rao. 2012. Poincaré wave-induced mixing in a large lake. Limnol. Oceanogr. **57**: 1201–1216. doi:10.4319/lo.2012.57.4.1201

Emery, W. J., and, R. E. Thomson. 1998. Data analysis methods in physical oceanography. Elsevier.

Frempong, E. 1983. Diel aspects of the thermal structure and energy budget of a small English lake. Freshwater Biol. **13**: 89–102. doi:10.1111/j.1365-2427.1983.tb00660.x

Gill, A. G. 1982. Atmosphere-ocean dynamics. Int. Geophys. Ser. **30**: 159–162

Gloor, M., A. Wuest, and D. M. Imboden. 2000. Dynamics of mixed bottom boundary layers and its implications for diapycnal transport in a stratified, natural water basin. J. Geophys. Res. Oceans **105**: 8629–8646. doi:10.1029/1999JC900303

Imberger, J. 1998. Flux paths in a stratified lake: A review. Physical processes in lakes and oceans. Coastal Estuarine Stud. **54**: 1–17. doi:10.1029/CE054p0001

Jassby, A., and, T. Powell. 1975. Vertical patterns of eddy diffusion during stratification in Castle Lake, California. Limnol. Oceanogr. **20**: 530–543. doi:10.4319/lo.1975.20.4.0530

Klink, J. 1999. dynmodes.m - ocean dynamic vertical modes. Woods Hole Science Center - SEA-MAT—Matlab Tools for Oceanographic Analysis. Available from http://woodshole.er.usgs.gov/operations/sea-mat/index.html.

Lhermitte, R., and, R. Serafin. 1984. Pulse-to-pulse coherent Doppler sonar signal processing techniques. J. Atmos. Oceanic Technol. **1**: 293–308. doi:10.1175/1520-0426(1984)001-0293:PTPCDS-2.0.CO;2

Lorke, A., B. Muller, M. Maerki, and A. Wuest. 2003. Breathing sediments. Limnol. Oceanogr. **48**: 2077–2085. doi:10.4319/lo.2003.48.6.2077

Lorke, A., and A. Wuest. 2005. Application of coherent ADCP for turbulence measurements in the bottom boundary layer. J. Atmos. Oceanic Technol. **22**: 1821–1828. doi:10.1175/JTECH1813.1

Lucas, N., J. H. Simpson, T. P. Rippeth, and, C. Old. 2014. Measuring dissipation via the structure function using a tethered ADCP. J Atmos. Oceanic Technol. **31**: 1826–1837. doi:10.1175/JTECH-D-13-00198.1

Maberly, S. C., and, J. A. Elliott. 2012. Insights from long-term studies in the Windermere catchment: External stressors, internal interactions and the structure and function of lake ecosystems. Freshw. Biol. **57**: 233–243. doi:10.1111/j.1365-2427.2011.02718.x

Miller, H., J. M. Bull, C. J. Cotterill, J. K. Dix, I. J. Winfield, A. E. S. Kemp, and R. B. Pearce. 2013. Lake bed geomorphology and sedimentary processes in glacial lake Windermere, UK. J Maps **9**: 299–312. doi:10.1080/17445647.2013.780986

Mortimer, C. H. 1952. Water movements in lakes during summer stratification: evidence from the distribution of temperature in Windermere. Philos. Trans. R. Soc. London **236**: 355–404. doi:10.1098/rstb.1952.0005

Mortimer, C. H. 1974. Lake hydrodynamics. Mitt. Int. Ver. Limnol. **20**: 124–197.

Munnich, M., A. Wuest, and D. M. Imboden. 1992. Observations of the second vertical modes of the internal seiche in an alpine lake. Limnol. Oceanogr. **37**: 1705–1719. doi:10.4319/lo.1992.37.8.1705

Ostrovsky, I., Y. Z. Yacobi, P. Walline, and I. Kalikhman. 1996. Seiche-induced mixing: Its impact on lake productivity. Limnol. Oceanogr. **41**: 323–332. doi:10.4319/lo.1996.41.2.0323

Ramsbottom, A. E. 1976. Depth charts of the Cumbrian Lakes. Freshw. Biol. Assoc. Scientific Publications, No. 33.

Sauvageot, H. 1992. Radar meteorology. Artech House.

Shih, L. H., J. R. Koseff, G. N. Ivey, and J. H. Ferziger. 2005. Parameterization of turbulent fluxes and scales using homogeneous sheared stably stratified turbulence simulations. J. Fluid Mech. **525**: 193–214. doi:10.1017/S0022112004002587

Simpson, J. H. 1981. The shelf-sea fronts: Implications of their existence and behaviour. Philos. Trans. R. Soc. Lond. **302**: 531–546. doi:10.1098/rsta.1981.0181

Simpson, J. H., P. Wiles, M. Ridgill, and M. Lewis. 2006. Direct Measurements of wind-induced internal motions in lakes using an ADCP. 10th European Workshop on Physical Processes in Natural Waters, Granada, Spain, University of Granada p. 31–40.

Simpson, J. H., P. J. Wiles, and B. J. Lincoln. 2011. Internal seiche modes and bottom boundary-layer dissipation in a temperate lake from acoustic measurements. Limnol. Oceanogr. **56**: 1893–1906. doi:10.4319/lo.2011.56.5.1893

Talling, J.F. 1999. Some English lakes as diverse and active ecosystems: A factual summary and source book. Freshwater Biological Association.

Thorpe, S. A. 1998. Some dynamical effects of internal waves and the sloping sides of lakes. Physical processes in lakes and oceans. Coastal Estuarine Stud. **54**: 441–460. doi:10.1029/CE054p0441

Thorpe, S. A. 2005. The turbulent ocean. Cambridge Univ. Press.

Wiles P. J., T. P. Rippeth, J. H. Simpson, and P. J. Hendricks. 2006. A novel technique for measuring the rate of turbulent dissipation in the marine environment. Geophys. Res. Lett. **33**: L21608. doi:10.1029/2006GL027050

Wuest, A., and A. Lorke. 2003. Small-scale hydrodynamics in lakes. Annu. Rev. Fluid Mech. **35**: 373–412. doi:10.1146/annurev.fluid.35.101101.161220

Wuest, A., G. Piepke, and D. C. Van Senden. 2000. Turbulent kinetic energy balance as a tool for estimating vertical diffusivity in wind-forced stratified waters. Limnol. Oceanogr. **45**: 1388–1400. doi:10.4319/lo.2000.45.6.1388

## Acknowledgments

We acknowledge the contribution made by Ben James of Centre for Ecology and Hydrology (CEH) in the deployment of instruments in Windermere from the R/V *John Lund*. Iestyn Woolway also helped in the supply of data from the CEH buoy. Thanks also to two anonymous referees for helpful comments.

*Submitted 20 March 2014*
*Revised 2 September 2014*
*Accepted 23 August 2014*

*Associate editor: Craig L. Stevens*